Thermophysical Properties of Mixtures of 2-Ethylhexanoic Acid and Ethanol

Babette Kunstmann, Maximilian Kohns,* and Hans Hasse

TU Kaiserslautern

Laboratory of Engineering Thermodynamics (LTD)

Erwin-Schrödinger-Str. 44

67663 Kaiserslautern, Germany

E-mail: maximilian.kohns@mv.uni-kl.de

Abstract

Mixtures of 2-ethylhexanoic acid (EHA) and ethanol are common solvents for precursor solutions in spray flame synthesis for the production of nanoparticles, however, no thermophysical data are available in the literature for these mixtures. Therefore, in this work, the density, viscosity, thermal conductivity, isobaric heat capacity, and self-diffusion coefficients of mixtures of EHA and ethanol were measured at atmospheric pressure and temperatures between 293.15 and 333.15 K. Additionally, isobaric vapor-liquid equilibria of the system were measured at pressures between 20 and 80 kPa. Empirical models were parametrized and are provided for all measured properties for convenient use in spray flame synthesis process simulations and related applications.

Introduction

Spray flame synthesis is a versatile aerosol process for the production of functional nanomaterials[1,2] for applications in several fields, including gas sensors,[3–5] energy,[6–8] biomedicine,[9,10] and catalysis.[11–13] In spray flame synthesis, a mixture of a combustible solvent and a metal-containing precursor – the so-called precursor solution – is sprayed into a flame. Mixtures of 2-ethylhexanoic acid (EHA) and ethanol are common solvents, especially in combination with metal nitrates as low-cost metal-containing precursors.[10,14–19]

The quality of the obtained nanomaterials depends strongly on the properties of the precursor solution. Thus, the thermophysical properties are necessary for gaining an improved process understanding and for the investigation by numerical techniques.[20–22] Property data are widely available for pure ethanol. For pure EHA, only some measurements of the vapor pressure,[23–31] enthalpy of vaporization,[29,32,33] and density at atmospheric pressure[32] as well as along the saturation line[29] have been reported. The viscosity was measured at 298.15, 313.15 and 373.15 K.[34] Furthermore, data on critical properties[29,35,36] as well as on the enthalpy of formation[32] and two-phase heat capacities[29] of EHA are available. For mixtures of EHA and ethanol, to the best of our knowledge, there are no data. Therefore, in this work, the density, viscosity, thermal conductivity, and isobaric heat capacity of pure EHA and ethanol and of mixtures of EHA and ethanol were measured at atmospheric pressure and temperatures between 293.15 and 333.15 K. Additionally, self-diffusion coefficient measurements at atmospheric pressure and temperatures between 298.15 and 333.15 K were performed. Isobaric vapor-liquid equilibria (VLE) were measured at pressures between 20 and 80 kPa. Empirical models were established and fit to the experimental data of all properties.

Experimental Section

Chemicals and Sample Preparation

The CAS registry numbers, suppliers, and purities of the chemicals used for sample preparation are given in Table 1. 1,4-Dioxane was used as an internal standard for gas chromatography (GC). Certified viscosity and density standards S6 and N.8 were purchased from Sigma-Aldrich. All chemicals were used without further purification. The samples were prepared gravimetrically using a Mettler-Toledo AG204 laboratory balance (specified standard uncertainty $u(m) = 0.0001$ g of the mass m) for sample masses smaller than 50 g and a Mettler-Toledo PR2003 Comparator laboratory balance (specified standard uncertainty $u(m) = 0.001$ g) for larger samples. A sample amount of approximately 10 ml is needed for the density and viscosity measurements at each temperature. Comparatively large samples are also necessary for the thermal conductivity and isobaric heat capacity measurements because the measurement cell has a volume of approximately 40 ml. The combined expanded uncertainty of the mole fraction of gravimetrically prepared samples is $U(x_{\mathrm{EtOH}}) = 0.001$ mol mol^{-1} ($k = 2$).

[Table 1 about here.]

Measurements

All measurement methods are as in our previous work.[37–40] Only the sample composition analysis for the VLE measurements was methodically different as explained below. In the supporting information, a comparison of the experimental results for the density and the viscosity of pure EHA from this work and the literature is presented in Figures S1 and S2. Figures S3 – S11 show a comparison of the experimental results for the pure component properties of ethanol from this work and the literature. As in our previous work,[39] good agreement is obtained in all cases. Furthermore, Figure S12 shows additional data for the self-diffusion coefficient of pure EHA as a function of temperature at temperatures between

298.15 and 353.15 K, for which no data for comparison are available in the literature. All measurements except for the VLE measurements were conducted at an atmospheric pressure of $p = 101.3$ kPa. The standard uncertainty of the pressure is $u(p) = 3$ kPa.

Density and Viscosity

A combined densimeter and viscosimeter from Anton Paar (SVM 3000) was used for density and viscosity measurements. The accuracy of its measurement results in the expected density and viscosity range was checked using density and viscosity standards S6 and N.8. The combined expanded uncertainty of the density measurements is $U(\rho) = 1$ kg m^{-3} ($k = 2$). The combined expanded uncertainty of the viscosity measurements is between $U(\eta) = 0.009$ mPa s ($k = 2$) and $U(\eta) = 0.146$ mPa s ($k = 2$) in the investigated viscosity range and is reported for each measurement result. The standard uncertainty of the temperature measurement specified by the manufacturer is $u(T) = 0.05$ K. Before the samples were introduced to the instrument, they were degassed in an ultrasonic bath for at least ten minutes.

Thermal Conductivity and Isobaric Heat Capacity

Thermal conductivity and isobaric heat capacity were measured with the hot-wire method. The instrument (LAMBDA, flucon fluid control GmbH) provides measurement results for the thermal conductivity λ and the thermal diffusivity a. From this, the isobaric heat capacity c_p can be calculated from eq. (1) if the sample density ρ is known:

$$c_p = \frac{\lambda}{a\ \rho} \tag{1}$$

The samples were thermostatted in a double-walled vessel. The instrument's temperature sensor was calibrated with a certified reference thermometer. The standard uncertainty of the temperature measurement in the measurement cell is estimated to be $u(T) = 0.1$ K.

The combined expanded relative uncertainties of the thermal conductivity and isobaric heat capacity measurements are $U_{\mathrm{rel}}(\lambda) = 0.04$ ($k = 2$) and $U_{\mathrm{rel}}(c_p) = 0.06$ ($k = 2$) respectively.

Self-Diffusion Coefficients

The self-diffusion coefficients of EHA and ethanol were determined by ^{1}H-NMR spectroscopy with pulsed field gradients following the procedures described in more detail by Bellaire et al..[41,42] The NMR spectrometer was equipped with an Ascend 400 magnet and an Avance III HD 400 console (both by Bruker) and provided a magnetic field strength of 9.4 T. The spectrometer's temperature sensor was calibrated using a Pt100 resistance thermometer. The standard uncertainty of the temperature measurement is estimated to be $u(T) = 0.1$ K. The self-diffusion coefficients were measured by a stimulated spin-echo technique with bipolar pulsed gradients using the pulse sequence *stebpgp1s*. The self-diffusion coefficients were calculated from the Stejskal-Tanner[43] equation:

$$\ln\left(\frac{I}{I_0}\right) = -D_i \varrho^2 \delta^2 g^2 \left(\Delta - \frac{1}{3}\delta - \frac{1}{2}\tau\right) \tag{2}$$

Here, I is the signal intensity, I_0 is the signal intensity without a gradient, D_i is the self-diffusion coefficient of component i, ϱ is the gyromagnetic ratio, δ is the duration of the application of the field gradient, g is the field gradient strength, Δ is the so-called diffusion time, and τ is a correction constant due to the use of bipolar gradients. The value of D_i was obtained from a fit of the natural logarithm of the relative intensity $\frac{I}{I_0}$ as a function of the squared field gradient g^2. For details see Refs. 41 and 42. The combined expanded uncertainty of the self-diffusion coefficient $U(D_i)$ from the fit to the experimental NMR data using eq. (2) depends strongly on the sample composition and the temperature and is specified here together with the measurement results.

Vapor-Liquid Equilibrium

Isobaric VLE of binary mixtures of ethanol and EHA were measured in a recirculating still glass apparatus, which is described in more detail in Ref. 44. The apparatus is an improved version of that designed by Rafflenbeul and Hartmann.[45] Measurements were performed at 20, 40, 60, and 80 kPa and temperatures up to 400 K. It is not possible to measure VLE at temperatures above 400 K with that setup. The pressure in the measurement cell was measured with a WIKA P-30 pressure sensor with a standard uncertainty of $u(p) = 0.05$ kPa. The equilibrium temperature was measured with a Pt100 resistance thermometer that was calibrated against a certified reference thermometer. While the calibrated thermometer provides a standard uncertainty better than 0.1 K, the uncertainty of the equilibrium temperature $u(T)$ is higher due to fluctuations during the measurement and is specified here together with the measurement results. The compositions of the liquid phase and the condensed gas phase were determined from an analysis of corresponding samples by gas chromatography (GC) using an Agilent 7890A GC system equipped with a flame ionization detector (FID) and a Zebron Phenomenex ZB-FFAP (30 m $\times$ 0.32 mm $\times$ 0.5 µm) column. In the GC measurements, 1,4-dioxane was used as an internal standard. The standard uncertainty of the ethanol mole fraction determined by GC is $u(x) = 0.01$ mol mol^{-1}.

Modeling

Density, Viscosity, Thermal Conductivity, and Isobaric Heat Capacity

Instead of modeling the results for the density ρ directly, a correlation for the molar volume v is presented, where

$$v = \frac{\bar{M}}{\rho}. \tag{3}$$

$\bar{M}$ is the average molar mass

$$\bar{M} = x_{\mathrm{EtOH}} M_{\mathrm{EtOH}} + x_{\mathrm{EHA}} M_{\mathrm{EHA}}, \tag{4}$$

where x_{EtOH} and x_{EHA} are the mole fractions of ethanol and EHA and M_{EtOH} and M_{EHA} are the molar masses of ethanol and EHA, respectively. The same modeling approach was used for the molar volume v, the viscosity η, the thermal conductivity λ, as well as for the molar isobaric heat capacity c_p. It is hence illustrated here using the symbol z for the studied property and $[z]$ for its unit, where $[v] = \mathrm{m^3\ mol^{-1}}$, $[\eta] = \mathrm{mPa\ s}$, $[\lambda] = \mathrm{W\ m^{-1}\ K^{-1}}$, $[c_p] = \mathrm{J\ mol^{-1}\ K^{-1}}$. The property z is described by the sum of an ideal mixture term and an excess term z^{E} (eq. (5)).

$$z/[z] = x_{\mathrm{EtOH}} z^{\mathrm{pure}}_{\mathrm{EtOH}} + x_{\mathrm{EHA}} z^{\mathrm{pure}}_{\mathrm{EHA}} + z^{\mathrm{E}} \tag{5}$$

Therein, the pure component properties z_i^{pure} and z^{E} are functions of the temperature T, since we only study properties at ambient pressure. The temperature dependence of the pure component properties z_i^{pure} is described by a polynomial (eq. (6)).

$$z_i^{\mathrm{pure}}/[z] = a_i + b_i\ T/\mathrm{K} + c_i\ (T/\mathrm{K})^2 \tag{6}$$

As an exception, an exponential temperature dependence (see eq. (7)) of the pure component viscosities η_i^{pure} is used:

$$\eta_i^{\text{pure}}/\text{mPa s} = a_i \exp\left(\frac{b_i}{T/\text{K}}\right) + c_i \tag{7}$$

In both cases, a_i, b_i, and c_i are adjustable parameters. The excess term is modeled by a Redlich-Kister-type correlation (see eq. (8)) with the adjustable parameters E, F, and G.

$$z^{\text{E}}/[z] = (E + F\ T/\text{K} + G\ x_{\text{EtOH}}x_{\text{EHA}})\ x_{\text{EtOH}}x_{\text{EHA}} \tag{8}$$

Self-Diffusion Coefficients

The self-diffusion coefficients were modeled using an empirical polynomial equation (eq. (9)) based on the approach of our previous work.[37] However, for describing the experimental data of the present work, a cubic term with respect to the mole fraction of ethanol x_{EtOH} was found to give better results than the quadratic term used in Ref. 37. Furthermore, a better description of the data is obtained if the mole fraction of ethanol x_{EtOH} is used instead of the mole fraction of the diffusing component x_i.

$$D_i/(10^{-9}\text{m}^2\ \text{s}^{-1}) = a_i + b_i\ T/\text{K} + (c_i + d_i\ T/\text{K})x_{\text{EtOH}} + (e_i + f_i\ T/\text{K})x_{\text{EtOH}}^3 \tag{9}$$

Vapor-Liquid Equilibrium

The VLE of binary mixtures of ethanol and EHA were modeled based on the extended Raoult's law

$$p_i^{\text{s}}\ x_i\ \gamma_i = p\ y_i, \tag{10}$$

where p_i^{s} is the vapor pressure of component i, x_i is the liquid phase mole fraction of component i, γ_i is the activity coefficient of component i, p is the total pressure, and y_i is the gas phase mole fraction of component i. The vapor pressures p_i^{s} were calculated from an Antoine-type equation with the empirical parameters A, B, and C which were obtained

from a fit to literature data.

$$\ln(p_i^{\mathrm{s}}/\mathrm{kPa}) = A_i + \frac{B_i}{T/\mathrm{K} + C_i} \tag{11}$$

The NRTL model (eq. (12)) was used for modeling the activity coefficients, which were assumed to be temperature-independent.

$$\ln \gamma_i = x_j^2 \left[\tau_{ji} \left(\frac{G_{ji}}{x_i + x_j G_{ji}} \right)^2 + \frac{\tau_{ij} G_{ij}}{\left(x_j + x_i G_{ij}\right)^2} \right] \tag{12}$$

Therein, G_{ij} is defined as

$$G_{ij} = \exp\left(-\alpha \tau_{ij}\right). \tag{13}$$

The adjustable parameters of the model are the two dimensionless interaction parameters τ_{ij}. The non-randomness parameter α was set to 0.3.

Fitting Procedure

Two different *python* solvers were employed in this work. *numpy.polyfit* was used to fit parameters of polynomials. Parameters for other equation types were obtained with *scipy.optimize.curve_fit*. For each property z, all N corresponding measured data points were considered simultaneously in the fit. The objective function was the sum of squared deviations between the measured and the calculated values for this property, as shown in eq. (14).

$$\mathrm{OF}_z = \sum_{j=1}^{N} \left(z_j^{\mathrm{exp}} - z_j^{\mathrm{cal}} \right)^2 \tag{14}$$

The objective function for the fit of the NRTL parameters was the sum of the squared deviations between measured and calculated pressures p_j. The results for the composition of the gas phase were not used as it contains predominantly the low-boiling component ethanol in the pressure range where experiments were possible.

Results and Discussion

The parameters a_i, b_i, and c_i for the correlations for the pure component properties (eqs. (6) and (7)) are given in Table 2. Table 3 lists the values of the parameters E, F, and G of the excess property correlations (eq. (8)). Table 4 lists the parameters for the empirical correlation (eq. (9)) for the self-diffusion coefficients. The parameters of the Antoine equation (11) for the pure component vapor pressures as obtained from a fit to literature data are given in Table 5. The NRTL parameters, which were determined from a fit of the present experimental data to the VLE model (eqs. (10), (12), and (13)), are given in Table 6.

[Table 2 about here.]

[Table 3 about here.]

[Table 4 about here.]

[Table 5 about here.]

[Table 6 about here.]

Density

The experimental results for the density of mixtures of EHA and ethanol are shown in Table 7 and are depicted in Figure 1 together with the model results. Pure EHA has a higher density than pure ethanol and thus, the mixture density decreases with increasing ethanol mole fraction x_{EtOH}. As expected, the density decreases with increasing temperature. The molar volume decreases almost linearly with increasing ethanol mole fraction and the molar excess volume is small compared to the overall molar volume. Thus, binary mixtures of ethanol and EHA behave approximately ideally with respect to the molar volume.

[Table 7 about here.]

[Figure 1 about here.]

Viscosity

Table 8 contains the experimental results for the mixture viscosities at different temperatures. Figure 2 depicts the measured and modeled viscosities as a function of the mixture composition at different temperatures. As expected, the viscosity decreases with increasing temperature. Pure EHA has a significantly higher viscosity than pure ethanol. Consequently, the viscosity of the mixtures of EHA and ethanol decreases with increasing ethanol content. The roughly linear relationship between viscosities at different compositions is rather unusual. The systems studied in our previous work[37–40] show a strong non-ideality of the mixture viscosity and a more complex model was necessary to describe the data.

[Table 8 about here.]

[Figure 2 about here.]

Thermal Conductivity

The results of the thermal conductivity measurements are given in Table 9 and are depicted in Figure 3 together with the model results. The thermal conductivities of both pure components and of all mixtures decrease with increasing temperature. Pure EHA has a lower thermal conductivity than pure ethanol. Thus, the mixture thermal conductivity increases with increasing ethanol mole fraction. A similar behavior is found, for example, for mixtures of ethanol with ethyl acetate[46] and with cyclohexane.[47]

[Table 9 about here.]

[Figure 3 about here.]

Isobaric Heat Capacity

The results of the isobaric heat capacity measurements are given in Table 10 and are depicted in Figure 4 together with the model results. Pure EHA has a significantly higher isobaric

heat capacity than pure ethanol. The isobaric heat capacity of mixtures of EHA and ethanol decreases almost linearly with the ethanol content and increases with increasing temperature. Hence, as for many mixtures investigated in our previous work,[37–40] the excess heat capacity is small.

[Table 10 about here.]

[Figure 4 about here.]

Self-Diffusion Coefficients

The results for the self-diffusion coefficients of pure ethanol and pure EHA as well as of ethanol and EHA in mixtures of ethanol and EHA are given in Tables 11 and 12, respectively. The experimental results together with those of the empirical correlation are depicted in Figure 5. As expected, since EHA is a larger molecule and has a higher viscosity than ethanol, its self-diffusion coefficient is generally lower than that of ethanol. Consequently, the self-diffusion coefficients of EHA and ethanol increase with increasing temperature and increasing ethanol content in the mixture. The strongly non-linear behavior with respect to the composition is in agreement with experimental and simulation results for other binary systems.[41,48]

[Table 11 about here.]

[Table 12 about here.]

[Figure 5 about here.]

Vapor-Liquid Equilibrium

The results of the VLE measurements are given in Table 13. Figure 6 depicts the experimental as well as the model results for the vapor-liquid equilibria of mixtures of ethanol and

EHA at the four different pressures considered in the present work. Due to the temperature limitation of 400 K of the experimental setup, it was not possible to obtain VLE data over the entire liquid phase composition range for $p > 40$ kPa. The system (EHA + ethanol) shows a zeotropic behavior with ethanol as the low-boiling and EHA as the high-boiling component. Due to the large difference in pure component boiling temperatures at all pressures, ethanol is the main component in the vapor phase over a wide concentration range. Thus, during the evaporation of an (EHA + ethanol) droplet in a hot atmosphere, as found in processes such as spray flame synthesis, ethanol will evaporate from the droplet surface preferentially. Significant amounts of EHA will only be found in the gas phase around an evaporating droplet once the ethanol mole fraction x_{EtOH} at the droplet surface is less than approximately 0.25 mol mol^{-1}, where the mixture boiling temperature increases steeply with decreasing ethanol content. Consequently, further evaporation of ethanol leads to a strong increase of the droplet temperature. If the liquid phase mass transfer is slow compared to the heat transfer, superheating in some parts of the droplet could occur and cause droplet micro-explosions.

[Table 13 about here.]

[Figure 6 about here.]

Conclusions

In the present work, thermophyiscal properties of mixtures of ethanol and EHA were measured: density, viscosity, thermal conductivity, isobaric heat capacity, self-diffusion coefficients of ethanol and EHA, and vapor-liquid equilibria. While the mixtures of EHA and ethanol behave almost ideally in terms of the molar volume and the isobaric heat capacity, for the viscosity, thermal conductivity, and self-diffusion coefficients important excess contributions were found. The VLE was found to be zeotropic with a wide-boiling behavior. Parameters for empirical correlations for all data were determined and are provided in this work. With the results of the present work, the integration of reliable property models for mixtures of EHA and ethanol in simulations of the spray flame synthesis process is made possible, which in turn enables detailed investigations to deepen process understanding and improve process designs.

Acknowledgement

This work was supported by the German Research Foundation (DFG) within the priority program SPP 1980 SPRAYSYN under the grants HA 1993/18-2 and KO 5844/2-2.

Supporting Information Available

The following files are available free of charge.

- SI_Thermophysical_Properties_EHA_Ethanol.pdf: Comparison of this work's results to literature data, additional self-diffusion coefficient data.

References

(1) Teoh, W. Y.; Amal, R.; Mädler, L. Flame spray pyrolysis: An enabling technology for nanoparticles design and fabrication. *Nanoscale* **2010**, *2*, 1324–1347.

(2) Pokhrel, S.; Mädler, L. Flame-made particles for sensors, catalysis, and energy storage applications. *Energy and Fuels* **2020**, *34*, 13209–13224.

(3) Samerjai, T.; Tamaekong, N.; Wetchakun, K.; Kruefu, V.; Liewhiran, C.; Siriwong, C.; Wisitsoraat, A.; Phanichphat, S. Flame-spray-made metal-loaded semiconducting metal oxides thick films for flammable gas sensing. *Sensors and Actuators, B: Chemical* **2012**, *171-172*, 43–61.

(4) Liewhiran, C.; Tamaekong, N.; Wisitsoraat, A.; Tuantranont, A.; Phanichphant, S. Ultra-sensitive H_2 sensors based on flame-spray-made Pd-loaded SnO_2 sensing films. *Sensors and Actuators B: Chemical* **2013**, *176*, 893–905.

(5) Punginsang, M.; Wisitsora-At, A.; Tuantranont, A.; Phanichphant, S.; Liewhiran, C. Effects of cobalt doping on nitric oxide, acetone and ethanol sensing performances of

FSP-made SnO_2 nanoparticles. *Sensors and Actuators, B: Chemical* **2015**, *210*, 589–601.

(6) Choi, S. H.; Kang, Y. C. Ultrafast synthesis of yolk-shell and cubic NiO nanopowders and application in lithium ion batteries. *ACS Applied Materials and Interfaces* **2014**, *6*, 2312–2316.

(7) Waser, O.; Hess, M.; Güntner, A.; Novák, P.; Pratsinis, S. E. Size controlled CuO nanoparticles for Li-ion batteries. *Journal of Power Sources* **2013**, *241*, 415–422.

(8) Meierhofer, F.; Li, H.; Gockeln, M.; Kun, R.; Grieb, T.; Rosenauer, A.; Fritsching, U.; Kiefer, J.; Birkenstock, J.; Mädler, L.; Pokhrel, S. Screening precursor–solvent combinations for $Li_4Ti_5O_12$ energy storage material using flame spray pyrolysis. *ACS Applied Materials and Interfaces* **2017**, *9*, 37760–37777.

(9) Lord, M. S.; Jung, M. S.; Teoh, W. Y.; Gunawan, C.; Vassie, J. A.; Amal, R.; Whitelock, J. M. Cellular uptake and reactive oxygen species modulation of cerium oxide nanoparticles in human monocyte cell line U937. *Biomaterials* **2012**, *33*, 7915–7924.

(10) Stodt, M. F.; Liu, C.; Li, S.; Mädler, L.; Fritsching, U.; Kiefer, J. Phase-selective laser-induced breakdown spectroscopy in flame spray pyrolysis for iron oxide nanoparticle synthesis. *Proceedings of the Combustion Institute* **2020**,

(11) Stark, W. J.; Maciejewski, M.; Mädler, L.; Pratsinis, S. E.; Baiker, A. Flame-made nanocrystalline ceria/zirconia: Structural properties and dynamic oxygen exchange capacity. *Journal of Catalysis* **2003**, *220*, 35–43.

(12) Chiarello, G. L.; Dozzi, M. V.; Scavini, M.; Grunwaldt, J. D.; Selli, E. One step flame-made fluorinated Pt/TiO_2 photocatalysts for hydrogen production. *Applied Catalysis B: Environmental* **2014**, *160-161*, 144–151.

(13) Liu, C.; Pokhrel, S.; Tessarek, C.; Li, H.; Schowalter, M.; Rosenauer, A.; Eickhoff, M.; Li, S.; Mädler, L. Rare-earth-doped $Y_4Al_2O_9$ nanoparticles for stable light-converting phosphors. *ACS Applied Nano Materials* **2020**, *3*, 699–710.

(14) Sotiriou, G. A.; Schneider, M.; Pratsinis, S. E. Color-tunable nanophosphors by codoping flame-made Y_2O_3 with Tb and Eu. *Journal of Physical Chemistry C* **2011**, *115*, 1084–1089.

(15) Harra, J.; Kujanpää, S.; Haapanen, J.; Juuti, P.; Mäkelä, J. M.; Hyvärinen, L.; Honkanen, M. Aerosol analysis of residual and nanoparticle fractions from spray pyrolysis of poorly volatile precursors. *AIChE Journal* **2017**, *63*, 881–892.

(16) Schneider, F.; Suleiman, S.; Menser, J.; Borukhovich, E.; Wlokas, I.; Kempf, A.; Wiggers, H.; Schulz, C. SpraySyn-A standardized burner configuration for nanoparticle synthesis in spray flames. *Review of Scientific Instruments* **2019**, *90*, 085108.

(17) Wei, J.; Li, S.; Ren, Y.; Zhang, Y.; Tse, S. D. Investigating the role of solvent formulations in temperature-controlled liquid-fed aerosol flame synthesis of YAG-based nanoparticles. *Proceedings of the Combustion Institute* **2019**, *37*, 1193–1201.

(18) Angel, S.; Neises, J.; Dreyer, M.; Friedel Ortega, K.; Behrens, M.; Wang, Y.; Arandiyan, H.; Schulz, C.; Wiggers, H. Spray-flame synthesis of La(Fe, Co)O_3 nanoperovskites from metal nitrates. *AIChE Journal* **2020**, *66*.

(19) Jüngst, N.; Smallwood, G. J.; Kaiser, S. A. Visualization and image analysis of droplet puffing and micro-explosion in spray-flame synthesis of iron oxide nanoparticles. *Experiments in Fluids* **2022**, *63*, 60.

(20) Rittler, A.; Deng, L.; Wlokas, I.; Kempf, A. M. Large eddy simulations of nanoparticle synthesis from flame spray pyrolysis. *Proceedings of the Combustion Institute* **2017**, *36*, 1077–1087.

(21) Martins, F. J.; Kirchmann, J.; Kronenburg, A.; Beyrau, F. Experimental investigation of axisymmetric, turbulent, annular jets discharged through the nozzle of the SPP1980 SpraySyn burner under isothermal and reacting conditions. *Experimental Thermal and Fluid Science* **2020**, *114*, 110052.

(22) Narasu, P.; Keller, A.; Kohns, M.; Hasse, H.; Gutheil, E. Numerical study of the evaporation and thermal decomposition of a single iron(III) nitrate nonahydrate/ethanol droplet. *International Journal of Thermal Sciences* **2021**, *170*, 107133.

(23) Levene, P.; Taylor, F. On Oxidation of tertiary hydrocarbons. *Journal of Biological Chemistry* **1922**, *54*, 351–362.

(24) Braun, J. V.; Manz, G. Die Umsetzung von Aldehyden mit Metallen und ihre katalytische Druck-Hydrierung. *Berichte der deutschen chemischen Gesellschaft (A and B Series)* **1934**, *67*, 1696–1712.

(25) Levene, P.; Rothen, A.; Meyer, G. Configurational relationship of members of disubstituted acetic and propionic acids containing an ethyl group. *Journal of Biological Chemistry* **1936**, *115*, 401–413.

(26) Whitmore, F. C.; Whitaker, J. S.; Mosher, W. A.; Breivik, O. N.; Wheeler, W. R.; Miner, C. S.; Sutherland, L. H.; Wagner, R. B.; Clapper, T. W.; Lewis, C. E.; Lux, A. R.; Popkin, A. H. Grignard Reductions. IX. Further studies on the reduction of acid halides. *Journal of the American Chemical Society* **1941**, *63*, 643–654.

(27) Weizmann, C.; Sulzbacher, M.; Bergmann, E. Reduction of alpha-beta-unsatured carbonyl-compounds by sodium-butoxide. *Journal of the Chemical Society* **1947**, *6*, 851–851.

(28) Weizmann, C.; Bergmann, E.; Sulzbacher, M. Further observations on the Guerbet reaction. *Journal of Organic Chemistry* **1950**, *15*, 54–57.

(29) Steele, W. V.; Chirico, R. D.; Knipmeyer, S. E.; Nguyen, A. Vapor pressure, heat capacity, and density along the saturation line, measurements for cyclohexanol, 2-cyclohexen-1-one, 1,2-dichloropropane, 1,4-di-tert-butylbenzene, (±)-2-ethylhexanoic Acid, 2-(methylamino)ethanol, perfluoro-n-heptane, and sulfolan. *Journal of Chemical and Engineering Data* **1997**, *42*, 1021–1036.

(30) Shen, Y.; Chen, Z.; Qiu, X.; Ma, Z.; Li, H.; Yang, J.; Ma, Y.; Gao, J.; Wang, Y. Isobaric vapor–liquid equilibrium measurements and calculations using nontraditional models for the association systems of ethyl acetate + 2-ethylhexanoic acid and propyl acetate + 2-ethylhexanoic acid at atmospheric pressure. *Journal of Chemical and Engineering Data* **2020**, *65*, 3482–3489.

(31) Ma, Y.; Gao, J.; Xu, D.; Zhang, L.; Wang, Y. Vapor-Liquid equilibrium study of binary mixtures of chloroform, 2-ethylhexanoic acid, and propylene glycol methyl ether at atmospheric pressure. *Journal of Chemical and Engineering Data* **2020**, *65*, 2271–2279.

(32) Stridh, G. Enthalpy of formation of 2-ethylhexanoic acid. *The Journal of Chemical Thermodynamics* **1976**, *8*, 193–194.

(33) Andereya, E.; Chase, J. D. The implications of carboxylic acid properties. *Chemical Engineering and Technology* **1990**, *13*, 304–312.

(34) Guo, H.; Smith, T. W.; Iglesias, P. The study of hexanoate-based protic ionic liquids used as lubricants in steel-steel contact. *Journal of Molecular Liquids* **2020**, *299*, 112208.

(35) Teja, A. S.; Rosenthal, D. J. Critical pressures and temperatures of twelve substances using a low residence time flow apparatus. AIChE Symposium Series. 1990; pp 133–137.

(36) Teja, A. S.; Anselme, M. J. Critical properties of thermally stable and unstable fluids. II. 1986 Results. AIChE Symposium Series. 1990; pp 115–121.

(37) Keller, A.; Wlokas, I.; Kohns, M.; Hasse, H. Thermophysical properties of mixtures of titanium(IV) isopropoxide (TTIP) and p-xylene. *Journal of Chemical and Engineering Data* **2020**, *65*, 869–876.

(38) Keller, A.; Wlokas, I.; Kohns, M.; Hasse, H. Thermophysical properties of solutions of iron(III) nitrate nonahydrate in mixtures of 1-propanol and water. *Journal of Chemical and Engineering Data* **2020**, acs.jced.0c00531.

(39) Keller, A.; Wlokas, I.; Kohns, M.; Hasse, H. Thermophysical properties of solutions of iron(III) nitrate-nonahydrate in mixtures of ethanol and water. *Journal of Chemical and Engineering Data* **2020**, *65*, 3519–3527.

(40) Keller, A.; Wlokas, I.; Kohns, M.; Hasse, H. Thermophysical properties of mixtures of titanium(IV) isopropoxide (TTIP) and 2-propanol (iPOH). *Journal of Chemical and Engineering Data* **2021**, *66*, 1296–1304.

(41) Bellaire, D.; Kiepfer, H.; Münnemann, K.; Hasse, H. PFG-NMR and MD simulation study of self-diffusion coefficients of binary and ternary mixtures containing cyclohexane, ethanol, acetone, and toluene. *Journal of Chemical and Engineering Data* **2020**, *65*, 793–803.

(42) Bellaire, D.; Großmann, O.; Münnemann, K.; Hasse, H. Diffusion coefficients at infinite dilution of carbon dioxide and methane in water, ethanol, cyclohexane, toluene, methanol, and acetone: A PFG-NMR and MD simulation study. *The Journal of Chemical Thermodynamics* **2022**, *166*, 106691.

(43) Stejskal, E. O.; Tanner, J. E. Spin diffusion measurements: Spin echoes in the presence of a time-dependent field gradient. *The Journal of Chemical Physics* **1965**, *42*, 288–292.

(44) Hasse, H. Dampf-Flüssigkeits-Gleichgewichte, Enthalpien und Reaktionskinetik in formaldehydhaltigen Mischungen. Ph.D. thesis, 1990.

(45) Rafflenbeul, L.; Hartmann, H. Eine dynamische Apparatur zur Bestimmung von Dampf-Fluessigkeits-Phasengleichgewichten. *Chem Technol* **1978**, *7*, 145–148.

(46) Qun-Fang, L.; Rui-Sen, L.; Dan-Yan, N.; Yu-Chun, H. Thermal conductivities of some organic solvents and their binary mixtures. *Journal of Chemical and Engineering Data* **1997**, *42*, 971–974.

(47) Baroncini, C.; Latini, G.; Pierpaoli, P. Thermal conductivity of organic liquid binary mixtures: Measurements and prediction method. *International Journal of Thermophysics* **1984**, *5*, 387–401.

(48) Guevara-Carrion, G.; Vrabec, J.; Hasse, H. Prediction of self-diffusion coefficient and shear viscosity of water and its binary mixtures with methanol and ethanol by molecular simulation. *The Journal of Chemical Physics* **2011**, *134*, 074508.

(49) Ambrose, D.; Sprake, C. Thermodynamic properties of organic oxygen compounds XXV. Vapour pressures and normal boiling temperatures of aliphatic alcohols. *The Journal of Chemical Thermodynamics* **1970**, *2*, 631–645.

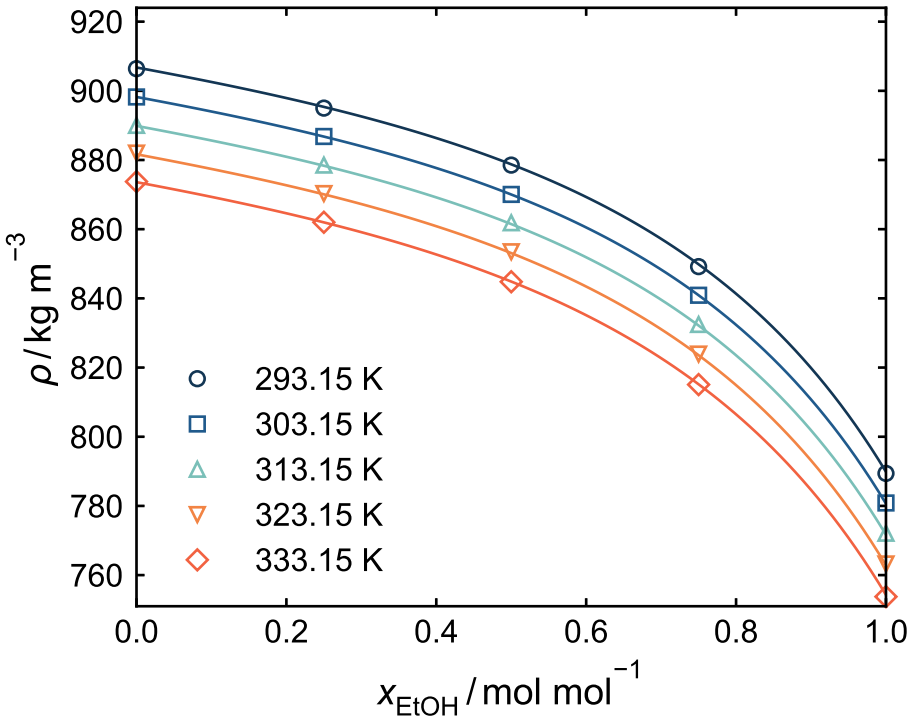

Figure 1: Density ρ of mixtures of EHA and ethanol at 101.3 kPa and different temperatures. Symbols are experimental results. Experimental uncertainties are within symbol size. Lines are empirical correlations, cf. eqs. (3)–(6), and (8), with parameters listed in Tables 2 and 3.

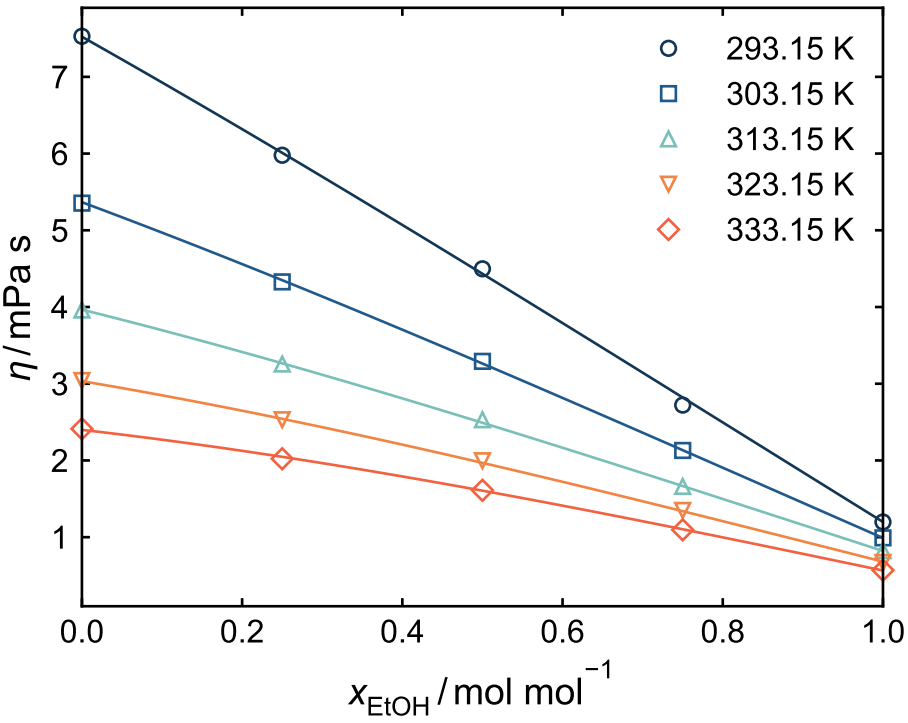

Figure 2: Viscosity η of mixtures of EHA and ethanol at 101.3 kPa and different temperatures. Symbols are experimental results. Experimental uncertainties are within symbol size. Lines are empirical correlations, cf. eqs. (5), (7), and (8), with parameters listed in Tables 2 and 3.

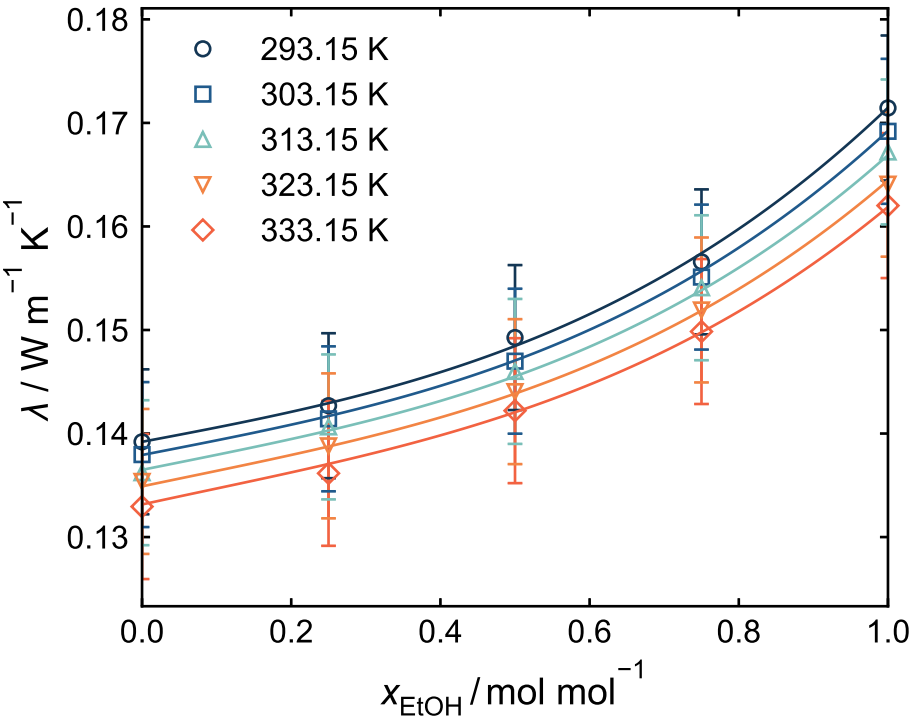

Figure 3: Thermal conductivity λ of mixtures of EHA and ethanol at 101.3 kPa and different temperatures. Symbols are experimental results. Error bars indicate the combined expanded uncertainty. Lines are empirical correlations, cf. eqs. (5), (6), and (8), with parameters listed in Tables 2 and 3.

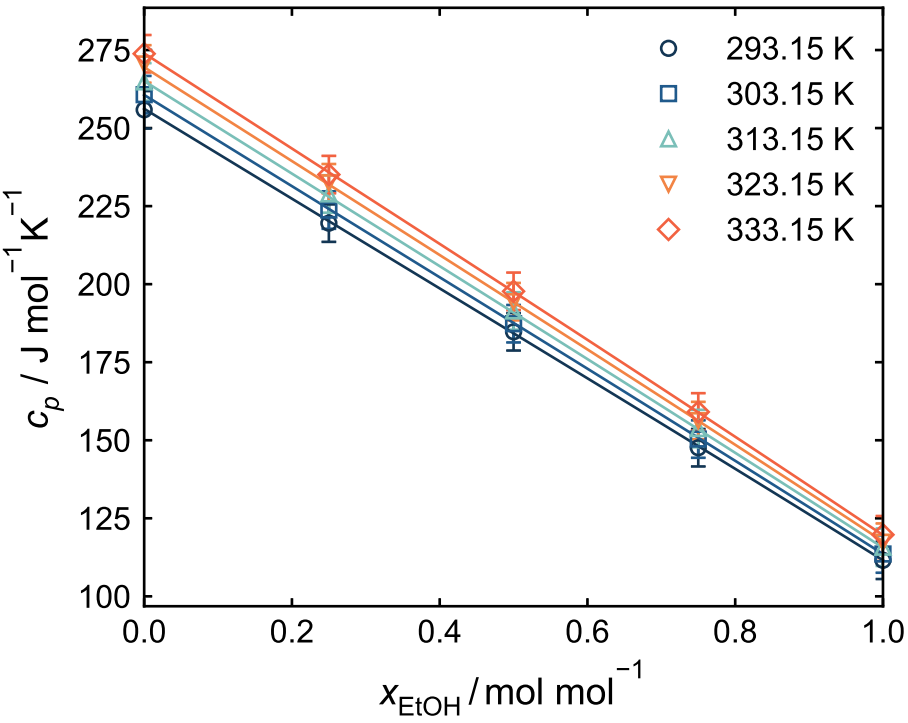

Figure 4: Isobaric heat capacity c_p of mixtures of EHA and ethanol at 101.3 kPa and different temperatures. Symbols are experimental results. Error bars indicate the combined expanded uncertainty. Lines are empirical correlations, cf. eqs. (5), (6), and (8), with parameters listed in Tables 2 and 3.

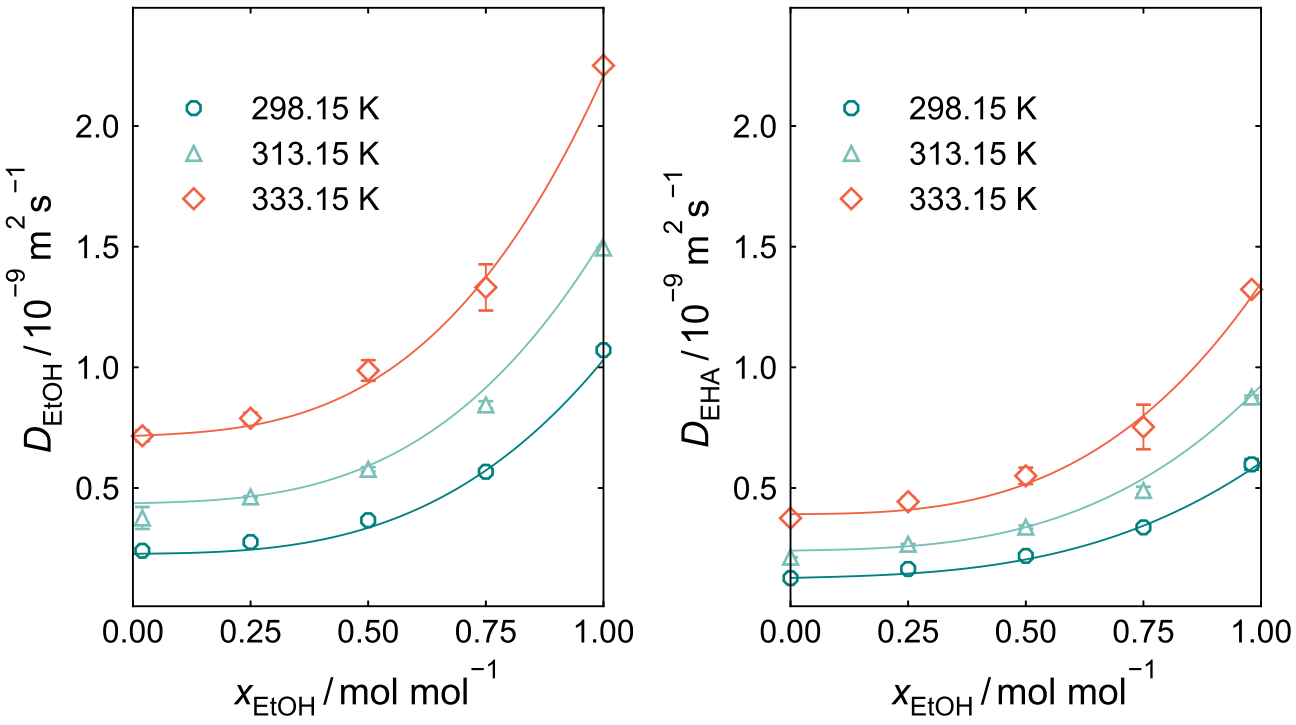

Figure 5: Self-diffusion coefficients of ethanol (left) and EHA (right) in mixtures of EHA and ethanol at 101.3 kPa and different temperatures. Symbols are experimental results. Error bars indicate the combined expanded uncertainty. Lines are empirical correlations, cf. eq. (9), with parameters listed in Table 4.

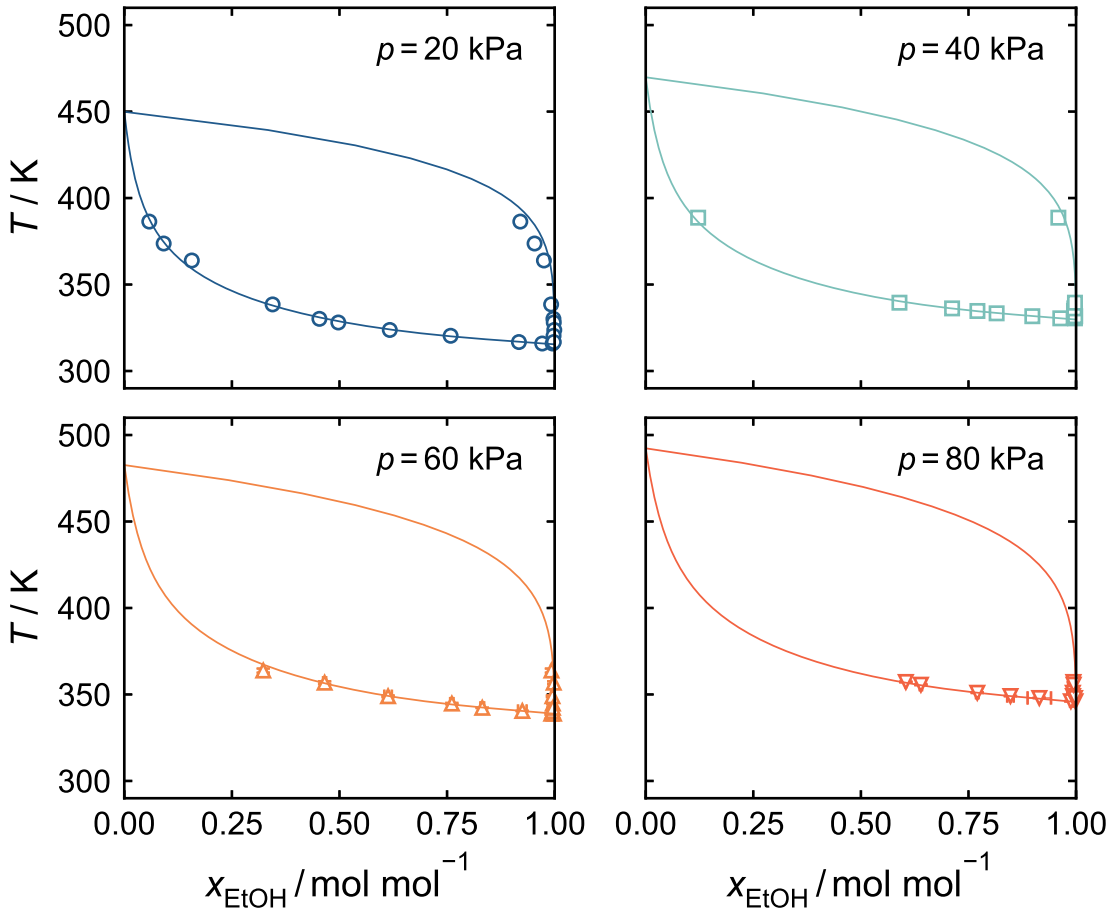

Figure 6: VLE of mixtures of EHA and ethanol. Symbols are experimental results. Error bars indicate the experimental standard uncertainty. Lines show modeling results using the extended Raoult's law with activity coefficients from NRTL, cf. eqs. (10), (11) and (12) and parameters from Tables 5 and 6.

Table 1: Chemical specification

	CAS reg. no.	supplier	mole fraction purity[a]
Ethanol (EtOH)	64-17-5	Supelco	≥ 0.999
2-Ethylhexanoic acid (EHA)	149-57-5	Sigma-Aldrich	0.998
1,4-Dioxane	123-91-1	Sigma-Aldrich	0.9993

[a] as specified by supplier

Table 2: Parameters of the correlations for the pure-component properties of EHA and ethanol

Property	Eq.	a	b	c
$v^{\text{pure}}_{\text{EtOH}}$ / m^3 mol^{-1}	(6)	3.8157×10^{-5}	6.8803×10^{-8}	0[a]
$\eta^{\text{pure}}_{\text{EtOH}}$ / mPa s	(7)	1.7032×10^{-2}	1.3167×10^{3}	-3.2105×10^{-1}
$\lambda^{\text{pure}}_{\text{EtOH}}$ / W m^{-1} K^{-1}	(6)	1.8982×10^{-1}	9.3203×10^{-5}	-5.3142×10^{-7}
$c^{\text{pure}}_{p,\text{EtOH}}$ / J mol^{-1} K^{-1}	(6)	5.2409×10^{1}	2.0175×10^{-1}	0[a]
$v^{\text{pure}}_{\text{EHA}}$ / m^3 mol^{-1}	(6)	1.1481×10^{-4}	1.5090×10^{-7}	0[a]
$\eta^{\text{pure}}_{\text{EHA}}$ / mPa s	(7)	7.4089×10^{-5}	3.3525×10^{3}	6.6045×10^{-1}
$\lambda^{\text{pure}}_{\text{EHA}}$ / W m^{-1} K^{-1}	(6)	1.0638×10^{-1}	3.4356×10^{-4}	-7.9010×10^{-7}
$c^{\text{pure}}_{p,\text{EHA}}$ / J mol^{-1} K^{-1}	(6)	1.2608×10^{2}	4.4382×10^{-1}	0[a]

[a] not needed and set to zero

Table 3: Parameters of the correlations for the excess properties of mixtures of EHA and ethanol (see eq. (8))

Property	E	F	G
v / $\mathrm{m^3\ mol^{-1}}$	-1.7280×10^{-7}	-5.0957×10^{-9}	-1.2009×10^{-6}
η / mPa s	-1.2335	5.1935×10^{-3}	-1.4577×10^{-1}
λ / $\mathrm{W\ m^{-1}\ K^{-1}}$	-6.9158×10^{-2}	1.4201×10^{-4}	-8.8192×10^{-3}
c_p / $\mathrm{J\ mol^{-1}\ K^{-1}}$	-1.0183×10^{1}	3.9976×10^{-2}	1.3266

Table 4: Parameters of the correlations for the self-diffusion coefficients (see eq. (9))

Component	a	b	c	d	e	f
Ethanol	-3.9337	1.3956×10^{-2}	-5.3178×10^{-1}	1.8497×10^{-3}	-4.5322	1.7832×10^{-2}
EHA	-2.1219	$7.544\,35 \times 10^{-3}$	3.0734×10^{-1}	-8.8196×10^{-4}	-3.9162	1.4590×10^{-2}

Table 5: Antoine parameters for EHA and ethanol obtained from fits of eq. (11) to the indicated literature data

Component	A	B	C	Ref.
Ethanol	1.6497×10^1	-3.5719×10^3	-5.0735×10^1	49
EHA	1.5235×10^1	-4.0666×10^3	-1.1761×10^2	29

Table 6: NRTL parameters obtained from a fit to the present experimental data

α	$\tau_{\mathrm{EtOH,EHA}}$	$\tau_{\mathrm{EHA,EtOH}}$
0.3	2.4197	−1.3430

Table 7: Results of the density measurements[a]

	ρ / kg m^{-3}				
	x_{EtOH} / mol mol^{-1}				
T / K	0	0.25	0.5	0.75	1
293.15	906.4	895.0	878.5	849.2	789.4
303.15	898.2	886.8	870.1	840.9	780.9
313.15	890.0	878.5	861.9	832.5	772.1
323.15	882.0	870.3	853.5	823.9	763.2
333.15	873.8	862.0	844.8	815.1	753.8

[a] Density ρ, liquid mole fraction x_{EtOH}, and temperature T at $p = 101.3$ kPa. The combined expanded uncertainties are $U(\rho) = 1$ kg m^{-3} ($k = 2$), $U(x_{\mathrm{EtOH}}) = 0.001$ mol mol^{-1} ($k = 2$), $u(p) = 3$ kPa, and $u(T) = 0.05$ K.

Table 8: Results of the viscosity measurements[a]

	η / mPa s ($U(\eta)$ / mPa s)				
	x_{EtOH} / mol mol^{-1}				
T / K	0	0.25	0.5	0.75	1
293.15	7.529 (0.146)	5.978 (0.050)	4.430 (0.039)	2.646 (0.025)	1.198 (0.010)
303.15	5.354 (0.046)	4.328 (0.037)	3.292 (0.028)	2.080 (0.020)	0.991 (0.009)
313.15	3.961 (0.034)	3.257 (0.028)	2.531 (0.021)	1.661 (0.014)	0.825 (0.013)
323.15	3.042 (0.026)	2.531 (0.021)	1.996 (0.017)	1.349 (0.011)	0.671 (0.025)
333.15	2.413 (0.021)	2.022 (0.017)	1.611 (0.015)	1.096 (0.027)	0.570 (0.042)

[a] Viscosity η, liquid mole fraction x_{EtOH}, and temperature T at $p = 101.3$ kPa. The combined expanded uncertainties are given in the table for $U(\eta)$ and $U(x_{\mathrm{EtOH}}) = 0.001$ mol mol^{-1} ($k = 2$), $u(p) = 3$ kPa, and $u(T) = 0.05$ K.

Table 9: Results of the thermal conductivity measurements[a]

	λ / W m^{-1} K^{-1}				
	x_{EtOH} / mol mol^{-1}				
T / K	0	0.25	0.5	0.75	1
293.15	0.139	0.143	0.149	0.157	0.171
303.15	0.138	0.141	0.147	0.155	0.169
313.15	0.136	0.141	0.146	0.154	0.167
323.15	0.135	0.139	0.144	0.152	0.164
333.15	0.133	0.136	0.142	0.150	0.162

[a] Thermal conductivity λ, liquid mole fraction x_{EtOH}, and temperature T at $p = 101.3$ kPa. The combined expanded relative uncertainty of the thermal conductivity is $U_{\mathrm{rel}}(\lambda) = 0.04$ ($k = 2$) and the other combined expanded uncertainties are $U(x_{\mathrm{EtOH}}) = 0.001$ mol mol^{-1} ($k = 2$), $u(p) = 3$ kPa, and $u(T) = 0.1$ K.

Table 10: Results of the isobaric heat capacity measurements[a]

	c_p / J mol^{-1} K^{-1}				
	x_{EtOH} / mol mol^{-1}				
T / K	0	0.25	0.5	0.75	1
293.15	256	220	185	148	112
303.15	261	224	187	150	114
313.15	265	229	191	154	116
323.15	271	233	194	156	117
333.15	274	235	198	159	120

[a] Isobaric heat capacity c_p, liquid mole fraction x_{EtOH}, and temperature T at $p = 101.3$ kPa. The combined expanded relative uncertainty of the isobaric heat capacity is $U_{\mathrm{rel}}(c_p) = 0.06$ ($k = 2$) and the other combined expanded uncertainties are $U(x_{\mathrm{EtOH}}) = 0.001$ mol mol^{-1} ($k = 2$), $u(p) = 3$ kPa, and $u(T) = 0.1$ K.

Table 11: Results of the self-diffusion coefficient measurements for ethanol[a]

	D_{EtOH} / 10^{-9} m^2 s^{-1} ($U(D_{\mathrm{EtOH}})$ / 10^{-9} m^2 s^{-1})				
	x_{EtOH} / mol mol^{-1}				
T / K	0.02	0.258	0.503	0.75	1
298.15	0.240 (0.001)	0.276 (0.001)	0.366 (0.001)	0.567 (0.001)	1.071 (0.001)
313.15	0.376 (0.045)	0.463 (0.003)	0.577 (0.009)	0.844 (0.016)	1.494 (0.002)
333.15	0.716 (0.023)	0.789 (0.023)	0.987 (0.043)	1.331 (0.096)	2.251 (0.006)

[a] Self-diffusion coefficient D_{EtOH}, liquid mole fraction x_{EtOH}, and temperature T at $p = 101.3$ kPa. The combined expanded uncertainties of the self-diffusion coefficient $U(D_{\mathrm{EtOH}})$ ($k = 2$) are given in the table and $U(x_{\mathrm{EtOH}}) = 0.001$ mol mol^{-1} ($k = 2$), $u(p) = 3$ kPa, and $u(T) = 0.1$ K.

Table 12: Results of the self-diffusion coefficient measurements for EHA[a]

	D_{EHA} / 10^{-9} m^2 s^{-1} ($U(D_{\mathrm{EHA}})$ / 10^{-9} m^2 s^{-1})				
	x_{EtOH} / mol mol^{-1}				
T / K	0	0.258	0.503	0.75	0.98
298.15	0.126 (0.001)	0.164 (0.001)	0.219 (0.002)	0.337 (0.002)	0.598 (0.022)
313.15	0.213 (0.001)	0.267 (0.002)	0.338 (0.007)	0.490 (0.016)	0.877 (0.006)
333.15	0.375 (0.001)	0.443 (0.018)	0.550 (0.034)	0.753 (0.092)	1.323 (0.007)

[a] Self-diffusion coefficient D_{EHA}, liquid mole fraction x_{EtOH}, and temperature T at $p = 101.3$ kPa. The combined expanded uncertainties of the self-diffusion coefficient $U(D_{\mathrm{EHA}})$ ($k = 2$) are given in the table and $U(x_{\mathrm{EtOH}}) = 0.001$ mol mol^{-1} ($k = 2$), $u(p) = 3$ kPa, and $u(T) = 0.1$ K.

Table 13: Results of the isobaric VLE measurements[a]

p / kPa	T / K	x_{EtOH} / mol mol^{-1}	y_{EtOH} / mol mol^{-1}
20	315.9	0.971	0.995
	316.7	0.917	0.998
	320.4	0.758	0.997
	323.7	0.617	0.999
	328.0	0.497	0.998
	330.2	0.453	0.997
	338.5	0.345	0.992
	363.9	0.157	0.975
	373.7	0.091	0.953
	386.4	0.058	0.920
40	330.5	0.963	0.997
	331.7	0.898	0.998
	333.3	0.815	0.998
	334.7	0.771	0.995
	336.2	0.712	0.996
	339.5	0.590	0.997
	388.7	0.122	0.959
60	338.9	0.992	0.998
	340.4	0.925	0.995
	342.3	0.832	0.996
	344.7	0.761	0.996
	349.0	0.613	0.995
	356.8	0.465	0.998
	363.8	0.323	0.993
80	346.1	0.988	0.999
	348.0	0.915	0.997
	349.1	0.848	0.993
	351.0	0.770	0.992
	355.7	0.639	0.994
	357.2	0.604	0.994

[a] Pressure p, temperature T, liquid phase mole fraction x_{EtOH}, and vapor phase mole fraction y_{EtOH}. The standard uncertainties are $u(p) = 0.05$ kPa, $u(T) = 1$ K, and $u(x_{\mathrm{EtOH}}) = u(y_{\mathrm{EtOH}}) = 0.01$ mol mol^{-1}

[Figure 7 about here.]

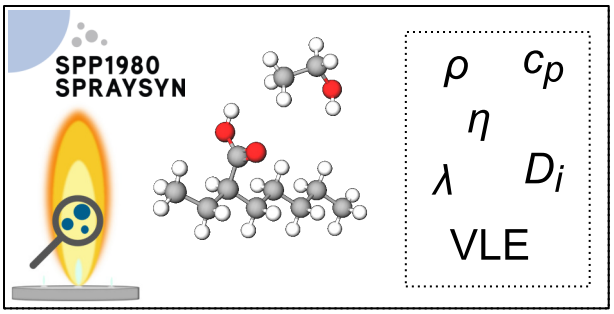

Figure 7: For Table of Contents Only